

PO-VINS: An Efficient Pose-Only LiDAR-Enhanced Visual-Inertial State Estimator

Hailiang Tang, Xiaoji Niu, Tisheng Zhang, Liqiang Wang, Guan Wang, and Jingnan Liu

Abstract—The pose-only (PO) visual representation has been proven to be equivalent to the classical multiple-view geometry, while significantly improving computational efficiency. However, its applicability for real-world navigation in large-scale complex environments has not yet been demonstrated. In this study, we present an efficient pose-only LiDAR-enhanced visual-inertial navigation system (PO-VINS) to enhance the real-time performance of the state estimator. In the visual-inertial state estimator (VISE), we propose a pose-only visual-reprojection measurement model that only contains the inertial measurement unit (IMU) pose and extrinsic-parameter states. We further integrated the LiDAR-enhanced method to construct a pose-only LiDAR-depth measurement model. Real-world experiments were conducted in large-scale complex environments, demonstrating that the proposed PO-VISE and LiDAR-enhanced PO-VISE reduce computational complexity by more than 50% and over 20%, respectively. Additionally, the PO-VINS yields the same accuracy as conventional methods. These results indicate that the pose-only solution is efficient and applicable for real-time visual-inertial state estimation.

Index Terms—State estimation, multi-sensor fusion navigation, visual-inertial navigation, factor graph optimization.

I. INTRODUCTION

Conventionally, the state-estimation problem in visual reconstruction and navigation is conducted by applying the bundle adjustment (BA) [1]. However, the high dimensional parameter space of visual landmarks significantly increases the computational complexity in solving the BA problem. In contrast, the dimension of the camera pose parameters is much less. Many methods have been presented to improve the efficiency of the BA, such as incremental BA [2], [3], fixed-lag smoother or sliding-window optimizer [4], [5], and preserving sparsity [6]. Nevertheless, too many computational resources have been used to estimate the parameter space of visual landmarks. Besides, only limited visual keyframes can be reserved to decrease the number of visual landmarks, leading to a poor accuracy in pose estimation.

Recently, the two-view imaging geometry has been proven to be equivalent to a pair of pose-only constraints decoupling camera poses from visual landmark parameters [7]. This work has been extended to the multiple-view imaging geometry [8]. The pose-only state estimation was conducted by adopting a pose adjustment rather than the BA, while the visual landmark parameters were analytically reconstructed from the obtained

This research is partly funded by the National Key Research and Development Program of China (No. 2020YFB0505803) and the National Natural Science Foundation of China (No. 41974024). (Corresponding author: Tisheng Zhang.)

Hailiang Tang, Liqiang Wang, and Guan Wang are with the GNSS Research Center, Wuhan University, Wuhan 430079, China (e-mail: thl@whu.edu.cn; wlq@whu.edu.cn; wanguan@whu.edu.cn).

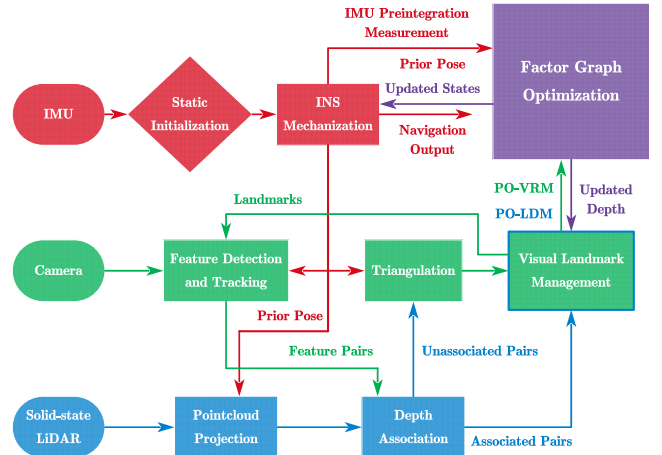


Fig. 1. System overview of PO-VINS. The PO-VRM denotes the pose-only visual-reprojection measurement in section III.B.2, and the PO-LDM denotes the pose-only LiDAR-depth measurement in section III.B.3.

camera poses [8]. The pose-only solution has demonstrated that computational efficiency is significantly improved by 2-4 orders of magnitude for three-dimensional scene reconstruction. However, the applicability of the pose-only solution for real-world navigation in large-scale complex environments has not yet been proven. Besides, the computational-efficiency improvement in a visual-inertial state estimator (VISE) is still known.

In this study, we incorporate the pose-only visual representation into the visual-inertial navigation system (VINS) to examine the accuracy and efficiency of the pose-only solution in large-scale complex environments. Moreover, the LiDAR-enhanced method can be seamlessly integrated into the pose-only state estimator by constructing a pose-only LiDAR-depth measurement model. The main contributions of our work are as follows:

- An efficient pose-only LiDAR-enhanced visual-inertial state estimator (PO-VINS) is presented. The pose-only visual-reprojection measurements, the pose-only LiDAR-depth measurements, and the IMU measurements are tightly fused within the factor graph optimization (FGO) framework to achieve a maximum-a-posteriori (MAP) estimation.
- A pose-only visual-reprojection measurement model is proposed, which contains only the inertial measurement unit

Xiaoji Niu is with the GNSS Research Center, Wuhan University, Wuhan 430079, China, the Hubei LuoJia Laboratory, Wuhan 430079, China, and the Artificial Intelligence Institute of Wuhan University, Wuhan 430079, China (email: xjniu@whu.edu.cn).

Tisheng Zhang and Jingnan Liu are with the GNSS Research Center, Wuhan University, Wuhan 430079, China, and the Hubei LuoJia Laboratory, Wuhan 430079, China (e-mail: zts@whu.edu.cn; jnliu@whu.edu.cn).

(IMU) pose and the extrinsic-parameter states.

- The LiDAR-enhanced method is integrated by constructing a pose-only LiDAR-depth measurement model to directly constrain the pose states.

- Real-world experiments were carried on in large-scale complex environments to evaluate the efficiency and accuracy of the proposed pose-only LiDAR-enhanced visual-inertial state estimator.

The remainder of this paper is organized as follows. We give an overview of the system pipeline in section II. The proposed pose-only LiDAR-enhanced VINS is presented in section III. The experiments and results are discussed in section IV for quantitative evaluation. Finally, we conclude the proposed PO-VINS.

II. SYSTEM OVERVIEW

The proposed PO-VINS is built upon our previous work LE-VINS [9] by incorporating the pose-only representation for visual-reprojection measurements and LiDAR-depth measurements. Fig. 1 depicts the system overview of the proposed PO-VINS. The front end of PO-VINS is the same as LE-VINS, and the works in this study are mainly in the back end, *i.e.* the state estimator. The INS is initialized by stationary conditions in this study. A visual-landmark management module is incorporated to construct the pose-only measurements. Specifically, the pose-only visual-reprojection measurements are established for all visual landmarks, without involving the visual-landmark states. In contrast, the inverse-depth parameterization [10] for visual landmarks is adopted in LE-VINS. For those visual landmarks with associated LiDAR depth, the pose-only LiDAR-depth measurements are proposed to directly constrain the pose states rather than the inverse-depth parameters of visual landmarks. Finally, the pose-only visual-reprojection measurements, the pose-only LiDAR-depth measurements, and the IMU measurements are tightly fused under the framework of FGO.

III. METHODOLOGY

This section presents the methodology of the proposed PO-VINS. We first derive the pose-only visual representation from the multiple-view geometry. Then, the pose-only LiDAR-enhanced visual-inertial state estimator is presented by incorporating the pose-only visual representation. Finally, the depth parameters for visual landmarks are analytically updated by the estimated poses to facilitate the follow-up processing.

A. Pose-Only Visual Representation

Consider a three-dimensional (3D) visual landmark in the world frame (w-frame) \mathbf{p}_w observed in several images, as depicted in Fig. 2. The origin of the camera frame (c-frame) is represented by \mathbf{O}_c . $\mathbf{p}_p = (x_p, y_p, 1)$ is the observed feature pixel coordinate in the normalized-camera frame (p-frame). The projection equation [1] of the 3D visual landmark \mathbf{p}_w in the p-frame can be written as

$$\mathbf{p}_p = \frac{1}{z_c} \mathbf{p}_c = \frac{1}{z_c} (\mathbf{R}_c^w)^{-1} (\mathbf{p}_w - \mathbf{p}_{wc}^w), \quad (1)$$

where $\mathbf{p}_c = (x_c, y_c, z_c)$ is the coordinate of the visual landmark in the c-frame; $\{\mathbf{p}_{wc}^w, \mathbf{R}_c^w\}$ is the camera pose in the w-frame.

For two images ς and η , we can derive the following equation from (1) as

$$z_{c_\varsigma} \mathbf{p}_{p_\eta} = z_{c_\varsigma} \mathbf{R}_{c_\varsigma}^{c_\eta} \mathbf{p}_{p_\varsigma} + \mathbf{p}_{c_\eta c_\varsigma}^{c_\eta}, \quad (2)$$

where $\{\mathbf{p}_{c_\eta c_\varsigma}^{c_\eta}, \mathbf{R}_{c_\varsigma}^{c_\eta}\}$ is the relative transformation from the c-frame c_ς to the c-frame c_η . Left multiply the anti-symmetric matrix $[\mathbf{p}_{p_\eta}]_\times$ on both sides of (2), and we can obtain

$$z_{c_\varsigma} [\mathbf{p}_{p_\eta}]_\times \mathbf{R}_{c_\varsigma}^{c_\eta} \mathbf{p}_{p_\varsigma} = -[\mathbf{p}_{p_\eta}]_\times \mathbf{p}_{c_\eta c_\varsigma}^{c_\eta}. \quad (3)$$

Taking the magnitude [8] in (3), the landmark depth z_{c_ς} in the c-frame c_ς can be written as

$$z_{c_\varsigma} = \frac{\|[\mathbf{p}_{p_\eta}]_\times \mathbf{p}_{c_\eta c_\varsigma}^{c_\eta}\|}{\theta_{\varsigma, \eta}}, \quad (4)$$

where $\theta_{\varsigma, \eta} = \|[\mathbf{p}_{p_\eta}]_\times \mathbf{R}_{c_\varsigma}^{c_\eta} \mathbf{p}_{p_\varsigma}\|$. Similarly, we can obtain

$$z_{c_\eta} = \frac{\|[\mathbf{R}_{c_\varsigma}^{c_\eta} \mathbf{p}_{p_\varsigma}]_\times \mathbf{p}_{c_\eta c_\varsigma}^{c_\eta}\|}{\theta_{\varsigma, \eta}}. \quad (5)$$

Hence, the pose-only constraint for the two-view imaging geometry in (2) can be written as

$$d_\eta^{(\varsigma, \eta)} \mathbf{p}_{p_\eta} = d_\varsigma^{(\varsigma, \eta)} \mathbf{R}_{c_\varsigma}^{c_\eta} \mathbf{p}_{p_\varsigma} + \mathbf{p}_{c_\eta c_\varsigma}^{c_\eta}. \quad (6)$$

The pose-only constraint in (6) has been proven to be equivalent to the two-view imaging geometry [7]. Supposing that ς and η are the left-based and right-based views [8] of the visual landmark \mathbf{p}_w , respectively, we can derive a set of constraints as

$$C(\varsigma, \eta) = \{d_i^{(\varsigma, i)} \mathbf{p}_{p_i} = d_\varsigma^{(\varsigma, \eta)} \mathbf{R}_{c_\varsigma}^{c_i} \mathbf{p}_{p_\varsigma} + \mathbf{p}_{c_i c_\varsigma}^{c_i}, i \neq \varsigma\}, \quad (7)$$

where i denotes another observed image, as shown in Fig. 2. The equation (7) is the pose-only representation for multiply-view geometry, and it can be proved that it is equivalent to the projection equation (1).

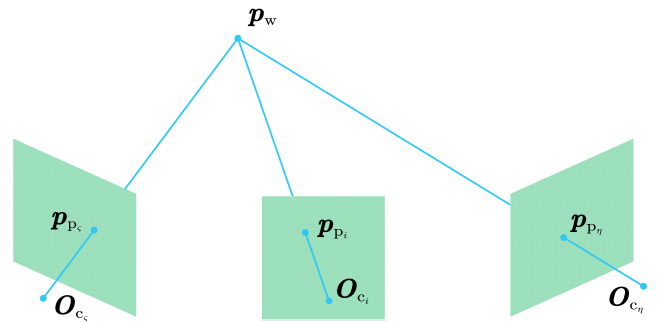


Fig. 2. An illustration of the multiply-view geometry. \mathbf{p}_w is a visual landmark in the world frame, observed by several images. The origin of the camera frame is represented by \mathbf{O}_c , and \mathbf{p}_p is the observed pixel coordinate in the normalized-camera frame.

Consequently, the pose-only measurements can be derived from (7). It should be noted that the images ς and η should construct the largest parallax of the landmark, and $\theta_{\varsigma,\eta}$ can be employed to represent the magnitude of the parallax [8]. In practice, the image ς is set to the first observed image or the image associated with LiDAR depth in PO-VINS. In addition, the image η is searched within the other images to meet the largest parallax.

B. Pose-Only State Estimator

The pose-only visual representation is incorporated into the LiDAR-enhanced visual-inertial state estimator in this part. Specifically, a pose-only visual-reprojection and a pose-only LiDAR-depth measurement models are presented. The pose-only measurements and the IMU-preintegration measurements are tightly fused within the FGO framework to perform a MAP estimation, as depicted in Fig. 3. Each time node in Fig. 3 represents that a visual keyframe is selected.

1) Formulation

The employed state estimator is a sliding-window optimizer [9]. The state vector \mathbf{X} in the sliding-window optimizer of PO-VINS can be defined as follow:

$$\begin{aligned} \mathbf{X} &= [\mathbf{x}_0, \mathbf{x}_1, \dots, \mathbf{x}_n, \mathbf{x}_c^b], \\ \mathbf{x}_k &= [\mathbf{p}_{wb_k}^w, \mathbf{q}_{b_k}^w, \mathbf{v}_{wb_k}^w, \mathbf{b}_{g_k}, \mathbf{b}_{a_k}], k \in [0, n], \\ \mathbf{x}_c^b &= [\mathbf{p}_{bc}^b, \mathbf{q}_c^b], \end{aligned} \quad (8)$$

where \mathbf{x}_k is the IMU state at each time node, including the position \mathbf{p}_{wb}^w , the attitude quaternion \mathbf{q}_b^w , and the velocity \mathbf{v}_{wb}^w in the w-frame, and the gyroscope biases \mathbf{b}_g and the accelerometer biases \mathbf{b}_a ; b denotes the IMU body frame (b-frame); n is the number of the IMU preintegration in the sliding window; \mathbf{x}_c^b is the camera-IMU extrinsic parameters. The attitude quaternion \mathbf{q} and the rotation matrix \mathbf{R} are equivalent for attitude parameterization [11]. The visual-landmark states are not contained in (8), and thus the state-estimator in PO-VINS is pose-only in terms of the visual-reprojection and LiDAR-depth measurements.

The following nonlinear optimization problem can be solved by minimizing the sum of the Mahalanobis norm of all measurements and the prior as

$$\min_{\mathbf{X}} \left\{ \sum_{l \in L} \left\| \mathbf{r}_V(\tilde{\mathbf{z}}_l^{V_{\varsigma,\eta,i}}, \mathbf{X}) \right\|_{\Sigma_l^{V_{\varsigma,\eta,i}}}^2 + \sum_{h \in [0,m]} \left\| \mathbf{r}_D(\tilde{\mathbf{z}}_h^{D_{\varsigma,\eta}}, \mathbf{X}) \right\|_{\Sigma_h^{D_{\varsigma,\eta}}}^2 \right. \\ \left. + \sum_{k \in [1,n]} \left\| \mathbf{r}_{Pre}(\tilde{\mathbf{z}}_{k-1,k}^{Pre}, \mathbf{X}) \right\|_{\Sigma_{k-1,k}^{Pre}}^2 + \left\| \mathbf{r}_p - \mathbf{H}_p \mathbf{X} \right\|^2 \right\}, \quad (9)$$

where \mathbf{r}_V are the residuals for the pose-only visual-reprojection measurements; L is the visual landmark map in the sliding window, and l is the landmark in the map; ς denotes the left-based keyframe of the landmark l ; η is the right-based keyframe; i is another observed keyframe of the landmark l ; \mathbf{r}_D are the residuals for the pose-only LiDAR-depth measurements, which directly constrain the pose states of the

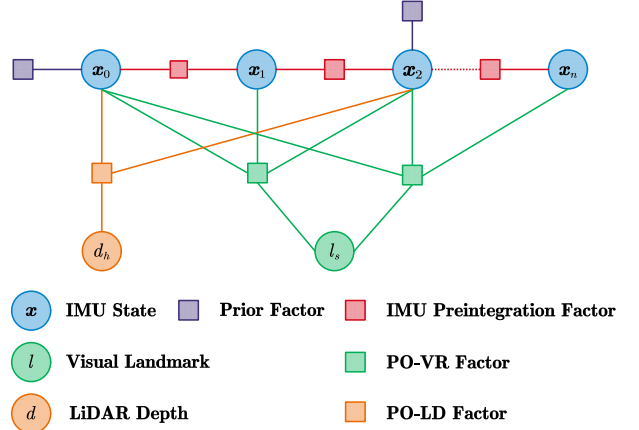


Fig. 3. FGO framework of PO-VINS. PO-VR denotes the pose-only visual-reprojection factor in section III.B.2, and PO-LD denotes the pose-only LiDAR-depth factor in section III.B.3. Here, we suppose a visual landmark l is observed in the states \mathbf{x}_0 , \mathbf{x}_1 , \mathbf{x}_2 , and \mathbf{x}_n , and is associated with LiDAR depth d . Besides, we suppose the left-based and right based views are happened in \mathbf{x}_0 and \mathbf{x}_2 .

keyframe ς and η ; \mathbf{r}_{Pre} are the residuals for the IMU-preintegration measurements; $\{\mathbf{r}_p, \mathbf{H}_p\}$ denotes the prior information from the marginalization [4], [12]. Ceres solver [13], an open-sourced library for modeling and solving large optimization problems, is adopted in PO-VINS. Specifically, the Levenberg-Marquardt algorithm is employed to solve the nonlinear least squares problem in (9).

2) Pose-Only Visual-Reprojection Measurement

From the pose-only representation (7), the landmark depth in the left-based visual keyframe ς can be expressed as the function of the camera poses as

$$\hat{d}_{\varsigma}^{(\varsigma,\eta)} \triangleq \frac{\left\| \begin{bmatrix} \tilde{\mathbf{p}}_{p_\eta} \end{bmatrix}_X \hat{\mathbf{p}}_{c_\eta}^{c_\eta} \right\|}{\hat{\theta}_{\varsigma,\eta}}, \quad (10)$$

$$\hat{\theta}_{\varsigma,\eta} = \left\| \begin{bmatrix} \tilde{\mathbf{p}}_{p_\eta} \end{bmatrix}_X \hat{\mathbf{R}}_{c_\varsigma}^{c_\eta} \tilde{\mathbf{p}}_{p_\varsigma} \right\|,$$

where $\hat{\cdot}$ and $\tilde{\cdot}$ denotes the estimated term and observed term, respectively. The relative pose $\{\hat{\mathbf{p}}_{c_\eta}^{c_\eta}, \hat{\mathbf{R}}_{c_\varsigma}^{c_\eta}\}$ can be written as

$$\begin{aligned} \hat{\mathbf{p}}_{c_\eta}^{c_\eta} &= (\hat{\mathbf{R}}_{c_\eta}^w)^{-1} (\hat{\mathbf{p}}_{wc_\eta}^w - \hat{\mathbf{p}}_{wc_\varsigma}^w), \\ \hat{\mathbf{R}}_{c_\varsigma}^{c_\eta} &= (\hat{\mathbf{R}}_{c_\eta}^w)^{-1} \hat{\mathbf{R}}_{c_\varsigma}^w. \end{aligned} \quad (11)$$

The camera pose $\{\mathbf{p}_{wc}^w, \mathbf{R}_c^w\}$ can be written as the function of the IMU pose and the extrinsic parameters as

$$\begin{aligned} \mathbf{p}_{wc}^w &= \mathbf{p}_{wb_k}^w + \mathbf{R}_{wb}^w \mathbf{p}_{bc}^b, \\ \mathbf{R}_c^w &= \mathbf{R}_{wb}^w \mathbf{R}_c^b, \end{aligned} \quad (12)$$

where $\{\mathbf{p}_{wb}^w, \mathbf{R}_{wb}^w\}$ is the IMU pose in the w-frame; $\{\mathbf{p}_{bc}^b, \mathbf{R}_c^b\}$ denotes the extrinsic parameters in (8).

For an observed keyframe i ($i \neq \varsigma, i \neq \eta$) of the landmark l , the pose-only visual-reprojection residuals can be derived from (7) as

$$\mathbf{r}_V(\tilde{\mathbf{z}}_i^{V, \eta}, \mathbf{X}) = (\mathbf{b}_1 \quad \mathbf{b}_2)^T (\hat{\mathbf{p}}_{p_i} - \tilde{\mathbf{p}}_{p_i}),$$

$$\hat{\mathbf{p}}_{p_i} = \frac{\hat{\mathbf{p}}_{c_i}}{\|\hat{\mathbf{p}}_{c_i}\|}, \quad (13)$$

where $\hat{\mathbf{p}}_{p_i}$ is the calculated pixel coordinate in the p-frame of the keyframe i ; \mathbf{b}_1 and \mathbf{b}_2 are two orthogonal bases that span the tangent plane of $\hat{\mathbf{p}}_{c_i}$. Here, $i \neq \eta$ are employed for better implementation using Ceres solver [13], which is a little different from the definition in (7). The covariance $\Sigma_i^{V, \eta, i}$ is propagated from the pixel plane onto the tangent plane. The calculated term $\hat{\mathbf{p}}_{c_i}$ can be written as

$$\hat{\mathbf{p}}_{c_i} = \hat{d}_i^{(\zeta, i)} \tilde{\mathbf{p}}_{p_i} = \hat{d}_\zeta^{(\zeta, \eta)} \hat{\mathbf{R}}_{c_\zeta}^{c_i} \tilde{\mathbf{p}}_{p_\zeta} + \hat{\mathbf{p}}_{c_\zeta}^{c_i}. \quad (14)$$

By considering (10), $\hat{\mathbf{p}}_{p_i}$ in (13) can be rewritten as

$$\hat{\mathbf{p}}_{p_i} = \frac{\hat{\theta}_{\zeta, \eta} \hat{\mathbf{p}}_{c_i}}{\hat{\theta}_{\zeta, \eta} \|\hat{\mathbf{p}}_{c_i}\|} = \frac{\hat{\mathbf{p}}_i}{\|\hat{\mathbf{p}}_i\|}$$

$$\hat{\mathbf{p}}_i = \left\| \left[\tilde{\mathbf{p}}_{p_\eta} \right]_{\mathbf{X}} \hat{\mathbf{p}}_{c_\eta}^{c_i} \right\| \hat{\mathbf{R}}_{c_\zeta}^{c_i} \tilde{\mathbf{p}}_{p_\zeta} + \left\| \left[\tilde{\mathbf{p}}_{p_\eta} \right]_{\mathbf{X}} \hat{\mathbf{R}}_{c_\zeta}^{c_i} \tilde{\mathbf{p}}_{p_\zeta} \right\| \hat{\mathbf{p}}_{c_\zeta}^{c_i}, \quad (15)$$

where $\hat{\mathbf{p}}_i$ is a coordinate in a scaled camera frame (only used for better representation); the relative pose $\{\hat{\mathbf{p}}_{c_\zeta}^{c_i}, \hat{\mathbf{R}}_{c_\zeta}^{c_i}\}$ can also be obtained from (11) and (12). Consequently, the calculated term $\hat{\mathbf{p}}_{p_i}$ is the function of the IMU poses $\{\hat{\mathbf{p}}_{w_b}^w, \hat{\mathbf{R}}_{b_c}^w\}$, $\{\hat{\mathbf{p}}_{w_b_i}^w, \hat{\mathbf{R}}_{b_i}^w\}$, and $\{\hat{\mathbf{p}}_{w_b_\eta}^w, \hat{\mathbf{R}}_{b_\eta}^w\}$, and the camera-IMU extrinsic parameters $\{\hat{\mathbf{p}}_{b_c}^b, \hat{\mathbf{R}}_c^b\}$. In other words, the visual-reprojection residuals in (13) is pose-only, without involving the visual landmark states, as shown in Fig. 3.

3) Pose-Only LiDAR-Depth Measurement

Similarly, the LiDAR-depth measurement model in [9] can be converted into a pose-only representation. By adopting the depth-association method in [9], we obtain the LiDAR depth observation in the visual c-frame as \tilde{d} . As mentioned in section III.A, the image ζ is set to the first observed image or the image associated with LiDAR depth, while the image η is searched within the other images to meet the largest parallax. In other words, the LiDAR-depth observation \tilde{d} is in the visual c-frame of the image ζ . Hence, the pose-only LiDAR-depth residual can be derived from (10) as

$$\mathbf{r}_D(\tilde{\mathbf{z}}_h^{D, \eta}, \mathbf{X}) = \frac{\left\| \left[\tilde{\mathbf{p}}_{p_\eta} \right]_{\mathbf{X}} \hat{\mathbf{p}}_{c_\eta}^{c_\zeta} \right\|}{\left\| \left[\tilde{\mathbf{p}}_{p_\eta} \right]_{\mathbf{X}} \hat{\mathbf{R}}_{c_\zeta}^{c_\eta} \tilde{\mathbf{p}}_{p_\zeta} \right\|} - \tilde{d}_h. \quad (16)$$

The covariance $\Sigma_h^{D, \eta}$ is set according to the distance threshold for the plane-checking algorithm in [9]. The LiDAR-depth residual in (16) is only the function of the IMU poses $\{\hat{\mathbf{p}}_{w_b}^w, \hat{\mathbf{R}}_{b_c}^w\}$ and $\{\hat{\mathbf{p}}_{w_b_\eta}^w, \hat{\mathbf{R}}_{b_\eta}^w\}$, and the camera-IMU extrinsic parameters $\{\hat{\mathbf{p}}_{b_c}^b, \hat{\mathbf{R}}_c^b\}$. Hence, the LiDAR-depth measurement in PO-VINS is also pose-only, which can directly constrain the

pose states, as depicted in Fig. 3. The LiDAR-depth measurement may directly affect the pose states in PO-VINS, rather than the visual-landmark states in LE-VINS, and thus the LiDAR-depth outlier may have more significant influence in Po-VINS. Hence, we have to add an extra outlier-culling algorithm to judge LiDAR-depth outliers before conducting the FOG.

4) IMU-Preintegration Measurement

We follow our previous work to employ the IMU preintegration in the state estimator [14]. The residuals of the IMU-preintegration measurement can be expressed as

$$\mathbf{r}_{Pre}(\tilde{\mathbf{z}}_{k-1, k}^{Pre}, \mathbf{X}) = \begin{pmatrix} \left(\mathbf{R}_{b_{k-1}}^w \right)^T \left(\mathbf{p}_{w_b_k}^w - \mathbf{p}_{w_b_{k-1}}^w - \mathbf{v}_{w_b_{k-1}}^w \Delta t_{k-1, k} \right) - \Delta \hat{\mathbf{p}}_{k-1, k}^{Pre} \\ -0.5 \mathbf{g}^w \Delta t_{k-1, k}^2 \\ \left(\mathbf{R}_{b_{k-1}}^w \right)^T \left(\mathbf{v}_{w_b_k}^w - \mathbf{v}_{w_b_{k-1}}^w - \mathbf{g}^w \Delta t_{k-1, k} \right) - \Delta \hat{\mathbf{v}}_{k-1, k}^{Pre} \\ 2 \left[\left(\mathbf{q}_{b_k}^w \right)^{-1} \otimes \mathbf{q}_{b_{k-1}}^w \otimes \hat{\mathbf{q}}_{k-1, k}^{Pre} \right]_v \\ \mathbf{b}_g - \mathbf{b}_{g_{k-1}} \\ \mathbf{b}_a - \mathbf{b}_{a_{k-1}} \end{pmatrix}, \quad (17)$$

where $\Delta \hat{\mathbf{p}}_{k-1, k}^{Pre}$, $\Delta \hat{\mathbf{v}}_{k-1, k}^{Pre}$, and $\hat{\mathbf{q}}_{k-1, k}^{Pre}$ are the position, velocity, and attitude preintegration measurements, respectively; \mathbf{g}^w are the gravity in the w-frame. The gyroscope biases \mathbf{b}_g and accelerometer biases \mathbf{b}_a in (17) are also included in the residuals for online estimation and correction. The covariance $\Sigma_{k-1, k}^{Pre}$ of the IMU-preintegration factor is derived from the noise propagation [14].

C. Depth Update for Visual Landmarks

The visual-landmark depth must be updated for the follow-up outlier-culling and feature-tracking processes. With the proposed pose-only visual-inertial state estimator, the visual-landmark depth can be analytically updated with the newly estimated camera poses. In [8], the visual landmarks are reconstructed by employing all the visual observations with the corresponding poses. However, we find that such processes will result in many landmarks being removed in the outlier-culling procedure. The visual-landmark depth has been implicitly determined by the left-based and right-based keyframes, *i.e.* ζ and η , as can be inferred from (10). Hence, the depth update for a visual landmark l can be written as

$$\hat{d} = \frac{\left\| \left[\tilde{\mathbf{p}}_{p_\eta} \right]_{\mathbf{X}} \hat{\mathbf{p}}_{c_\eta}^{c_\zeta} \right\|}{\left\| \left[\tilde{\mathbf{p}}_{p_\eta} \right]_{\mathbf{X}} \hat{\mathbf{R}}_{c_\zeta}^{c_\eta} \tilde{\mathbf{p}}_{p_\zeta} \right\|}, \quad (18)$$

where \hat{d} is defined in the left-based keyframe ζ , which is the same as in (10). It should be noted that the depth update in (18) is adopted mainly to adapt to the existing outlier-culling algorithm in [9], [15].

IV. EXPERIMENTS AND RESULTS

A. Equipment Setup and Configurations

The LE-VINS dataset, *i.e.* *Experiment-1* and *Experiment-2*,

are adopted for quantitative evaluation. The trajectory lengths of *Experiment-1* and *Experiment-2* are 2560 m (1820 s) and 2539 m (1805 s), respectively. The employed sensors include the camera (with a resolution of 1280×1024), the industrial-grade MEMS IMU (with the gyroscope bias instability of $2^\circ/\text{hr}$), and the solid-state LiDAR (Livox Mid-70).

The modified version of IC-VINS in [15] and LE-VINS in [9] are employed for accuracy and efficiency comparison. The inverse-depth parameterization [10] for visual landmarks is adopted in IC-VINS and LE-VINS. The INS is initialized with stationary conditions for the modified IC-VINS, the modified LE-VINS, and the proposed PO-VINS. For convenience, PO-VINS-WO denotes the proposed pose-only visual-inertial state estimator without LiDAR enhancement. We use a max of 150 visual feature points and 10 IMU-preintegration factors in the sliding window for these systems. They are all run on a desktop PC (AMD CPU R7-3700X with 32 GB RAM, and NVIDIA GPU RTX2060 with 6 GB RAM) under the framework of ROS. The optical-flow algorithm is run on the NVIDIA GPU RTX2060, while other processes are run on the CPU. We read the ROS data bag rather than played the data bag to fully evaluate the efficiency of the systems.

The absolute and relative pose errors [16] were adopted for quantitative evaluation. Specifically, the relative error over the sub-sequences of the length of 25m, 50m, 100m, and 200m are employed to evaluate the short-term and long-term accuracy.

B. Evaluation of the Accuracy

1) Comparison of the Absolute Error

We calculate the absolute error of the four navigation systems in the two large-scale datasets, as shown in Table I. For pure VINS, PO-VINS-WO almost yields the same accuracy as IC-VINS. The LiDAR-enhanced methods indicate improved accuracy for PO-VINS and LE-VINS in *Experiment-1*, while degraded accuracy in *Experiment-2*. Besides, PO-VINS exhibits a larger translation error in *Experiment-1*, compared to LE-VINS. As the visual-inertial estimator in IC-VINS or PO-VINS has already achieved superior, the LiDAR-enhanced method shows limited improvement in terms of absolute accuracy [9]. Hence, the absolute error results are acceptable for PO-VINS. All in all, the proposed pose-only LiDAR-enhanced visual-inertial state estimator demonstrates nearly the same accuracy compared to the conventional state estimator.

2) Comparison of the Relative Error

We further calculate the relative error to fully evaluate the local consistency or robustness [17] of the proposed PO-VINS. The relative rotation error (RRE) and the relative translation error (RTE) are exhibited in Table II. The front end includes feature detection, feature tracking, LiDAR-depth association, and *et. al.* The back end, *i.e.* state estimator, includes the sliding-windows optimization and marginalization. Compared to IC-VINS, PO-VINS-WO indicates a larger short-term error in terms of the RTEs of 25 m, especially in *Experiment-1*. The LiDAR enhancement can significantly improve the short-term accuracy for both LE-VINS and PO-VINS. Besides, PO-VINS only exhibits a little larger relative error, especially for the RTEs over 25 m. In conclusion, the pose-only visual-inertial

TABLE I
ABSOLUTE ROTATION AND ABSOLUTE TRANSLATION ERROR

ARE / ATE (deg / m)	<i>Experiment-1</i>	<i>Experiment-2</i>
IC-VINS	0.607 / 2.163	0.267 / 1.128
LE-VINS	0.436 / 1.614	0.342 / 1.317
PO-VINS-WO	0.498 / 2.115	0.327 / 1.088
PO-VINS	0.480 / 1.943	0.469 / 1.251

PO-VINS-WO denotes the proposed pose-only visual-inertial state estimator without LiDAR enhancement.

TABLE II
RELATIVE ROTATION AND RELATIVE TRANSLATION ERROR

RRE / RTE (deg / %)	25 m	50 m	100 m	200 m
<i>Experiment-1</i>				
IC-VINS	0.12 / 1.08	0.17 / 0.81	0.25 / 0.66	0.38 / 0.56
LE-VINS	0.11 / 0.66	0.15 / 0.62	0.22 / 0.57	0.37 / 0.53
PO-VINS-WO	0.12 / 1.40	0.17 / 1.07	0.25 / 0.83	0.40 / 0.67
PO-VINS	0.12 / 0.76	0.18 / 0.73	0.28 / 0.70	0.47 / 0.67
<i>Experiment-2</i>				
IC-VINS	0.10 / 0.79	0.13 / 0.58	0.17 / 0.46	0.23 / 0.35
LE-VINS	0.10 / 0.46	0.12 / 0.40	0.17 / 0.36	0.25 / 0.31
PO-VINS-WO	0.11 / 0.87	0.15 / 0.67	0.21 / 0.52	0.27 / 0.39
PO-VINS	0.10 / 0.52	0.14 / 0.46	0.21 / 0.41	0.35 / 0.39

state estimator may result in poor robustness in terms of short-term accuracy. Nevertheless, the proposed PO-VINS demonstrates almost the same robustness compared to the conventional state estimator with the LiDAR enhancement.

C. Evaluation of the Efficiency

As the motivation of this paper is to improve the computational efficiency of the state estimator, we evaluate the efficiency of the proposed PO-VINS. The running time and running speed results are shown in Table III. The average time of the front end is almost the same for the pose-only methods and non-pose-only methods, as the differences for these systems are mainly in the back end.

In terms of the state estimator, the running time of PO-VINS-WO decreases by 53.5% and 52.6% in the two experiments, compared to IC-VINS. The results are not unexpected, as the state estimator is not large-scale in the sliding-window optimizer. Specifically, there are $15 * 11 = 165$ dimensions of the IMU states for the window size of 10, as the IMU states are 15 dimensions at each time node. However, there are usually 100~200 visual landmarks in the sliding window according to our experience, when we detect a max of 150 feature points in each image. In other words, if we use the inverse-depth parameterization for visual landmarks, there are only 100~200 dimensions for visual landmarks. The visual-landmark states are almost the same as IMU states, and occupy almost only a

TABLE III
RUNNING TIME AND RUNNING SPEED

Time	Average front end (ms)	Average back end (ms)	Running Time (s)	Running speed
<i>Experiment-1 (1820 s)</i>				
IC-VINS	7.17	24.32	411	4.4×
LE-VINS	12.34	25.54	451	4.0×
PO-VINS-WO	7.16	11.31	331	5.5×
PO-VINS	12.11	19.14	409	4.5×
<i>Experiment-2 (1805 s)</i>				
IC-VINS	7.29	22.92	408	4.4×
LE-VINS	12.19	24.19	446	4.1×
PO-VINS-WO	7.22	10.86	329	5.5×
PO-VINS	12.22	19.16	418	4.3×

The front end includes the feature detection, feature tracking, LiDAR-depth association, and *et. al.* The back end, *i.e.* state estimator, includes the sliding-windows optimization and marginalization.

half of the total states. Consequently, it is satisfied that the computational complexity for the state estimator has decreased by more than 50%.

Besides, the average back-end running time of PO-VINS decreases by 25.1% and 20.8% compared to LE-VINS. By incorporating the LiDAR depth, PO-VINS exhibits less efficiency improvement compared to PO-VINS-WO. The result is that the pose-only LiDAR-depth constraints are direct to the pose states, but we have not refined the initial poses using the LiDAR depth before conducting the FGO. Specifically, the initial poses are obtained from the INS mechanization [9]. Such inconsistency between the LiDAR depth and the initial poses results in more iterations during the FGO. Adopting a pose-refinement algorithm using the LiDAR depth, such as EPnP [18] and FGO, may solve this problem and further improve computational efficiency.

The running-speed results indicate that PO-VINS-WO can run at 5.5× speeds, while 4.4× speeds for IC-VINS. With the LiDAR enhancement, PO-VINS can also run at more than 4.3× speeds and LE-VINS can almost run at 4.0× speeds. The results demonstrate that the proposed pose-only state can significantly improve computational efficiency.

V. CONCLUSIONS AND DISCUSSIONS

This study proposes an efficient pose-only LiDAR-enhanced visual-inertial state estimator. We present a pose-only visual-reprojection measurement model and a pose-only LiDAR-depth measurement model in the VISE. The pose-only measurements and the IMU measurements are tightly fused within the FGO framework to perform a MAP estimation. Real-world experiments indicate that the proposed PO-VINS achieve the same accuracy compared to the conventional methods while improving the computational efficiency notably. Specifically, the computational complexity is reduced by more than 50% and

more than 20% for the proposed PO-VISE and the LiDAR-enhanced PO-VISE, respectively.

The pose-only solution is implemented by using the camera poses to implicitly represent the visual-landmark depth, and thus the visual-landmark states can be removed from the state estimator. The decreased dimensions in the state estimator result in improved efficiency when solving the nonlinear optimization problem. Though the pose-only representation has been proven to be equivalent to the multiple-view geometry theoretically, the impact of the outliers or biased observations cannot be neglected. Such influences may be more significant in visual complex environments. Consequently, the current implementation of PO-VINS still should be improved a lot, and the following issues should be considered.

- 1) A more appropriate and applicable visual outlier-culling algorithm for pose-only solution. The current implementation is based on the reprojection error, which utilizes the visual-landmark depth or coordinates. Hence, we have to adopt the depth-update formulation in (18) to adapt such a reprojection-based outlier-culling algorithm.
- 2) An initial pose refinement algorithm when incorporating the LiDAR depth. As the pose-only LiDAR-depth constraints are direct to the pose states, the initial pose estimation must be refined to further decrease the iterations and improve the efficiency.
- 3) A pose-only visual-reprojection implementation for the visual landmarks with only two observations. The current implementation must include more than three observations for a visual landmark, mainly because of the implementation using Ceres solver, resulting in a loss of information.

Despite these addressed issues, the results of this study indicate that the pose-only solution is efficient and applicable for visual-inertial state estimation. Our work demonstrates that the pose-only representation is meaningful for real-time visual-inertial navigation, not just for offline 3D reconstruction.

REFERENCES

- [1] R. Hartley and A. Zisserman, *Multiple View Geometry in Computer Vision, Second Edition*. Cambridge university press, 2003.
- [2] H. Liu, M. Chen, G. Zhang, H. Bao, and Y. Bao, "ICE-BA: Incremental, Consistent and Efficient Bundle Adjustment for Visual-Inertial SLAM," in *2018 IEEE/CVF Conference on Computer Vision and Pattern Recognition*, Salt Lake City, UT: IEEE, Jun. 2018, pp. 1974–1982. doi: 10.1109/CVPR.2018.00211.
- [3] M. Kaess, H. Johannsson, R. Roberts, V. Ila, J. J. Leonard, and F. Dellaert, "iSAM2: Incremental smoothing and mapping using the Bayes tree," *Int. J. Robot. Res.*, vol. 31, no. 2, pp. 216–235, Feb. 2012, doi: 10.1177/0278364911430419.
- [4] S. Leutenegger, S. Lynen, M. Bosse, R. Siegwart, and P. Furgale, "Keyframe-based visual-inertial odometry using nonlinear optimization," *Int. J. Robot. Res.*, vol. 34, no. 3, pp. 314–334, Mar. 2015, doi: 10.1177/0278364914554813.
- [5] T. Qin, P. Li, and S. Shen, "VINS-Mono: A Robust and Versatile Monocular Visual-Inertial State Estimator," *IEEE Trans. Robot.*, vol. 34, no. 4, pp. 1004–1020, Aug. 2018, doi: 10.1109/TRO.2018.2853729.
- [6] E. D. Nerurkar, K. J. Wu, and S. I. Roumeliotis, "C-KLAM: Constrained keyframe-based localization and mapping," in *2014 IEEE International Conference on Robotics and Automation (ICRA)*, May 2014, pp. 3638–3643. doi: 10.1109/ICRA.2014.6907385.

- [7] Q. Cai, Y. Wu, L. Zhang, and P. Zhang, “Equivalent Constraints for Two-View Geometry: Pose Solution/Pure Rotation Identification and 3D Reconstruction,” *Int. J. Comput. Vis.*, vol. 127, no. 2, pp. 163–180, Feb. 2019, doi: 10.1007/s11263-018-1136-9.
- [8] Q. Cai, L. Zhang, Y. Wu, W. Yu, and D. Hu, “A Pose-Only Solution to Visual Reconstruction and Navigation,” *IEEE Trans. Pattern Anal. Mach. Intell.*, vol. 45, no. 1, pp. 73–86, Jan. 2023, doi: 10.1109/TPAMI.2021.3139681.
- [9] H. Tang, X. Niu, T. Zhang, L. Wang, and J. Liu, “LE-VINS: A Robust Solid-State-LiDAR-Enhanced Visual-Inertial Navigation System for Low-Speed Robots,” *IEEE Trans. Instrum. Meas.*, vol. 72, pp. 1–13, 2023, doi: 10.1109/TIM.2023.3260279.
- [10] J. Civera, A. J. Davison, and J. M. M. Montiel, “Inverse Depth Parametrization for Monocular SLAM,” *IEEE Trans. Robot.*, vol. 24, no. 5, pp. 932–945, Oct. 2008, doi: 10.1109/TRO.2008.2003276.
- [11] J. Sola, “Quaternion kinematics for the error-state Kalman filter,” *ArXiv Prepr. ArXiv171102508*, 2017.
- [12] J. Engel, V. Koltun, and D. Cremers, “Direct Sparse Odometry,” *IEEE Trans. Pattern Anal. Mach. Intell.*, vol. 40, no. 3, pp. 611–625, Mar. 2018, doi: 10.1109/TPAMI.2017.2658577.
- [13] Agarwal, Sameer, Mierle, Keir, and The Ceres Solver Team, “Ceres Solver.” Mar. 2022. [Online]. Available: <https://github.com/ceres-solver/ceres-solver>
- [14] H. Tang, T. Zhang, X. Niu, J. Fan, and J. Liu, “Impact of the Earth Rotation Compensation on MEMS-IMU Preintegration of Factor Graph Optimization,” *IEEE Sens. J.*, vol. 22, no. 17, pp. 17194–17204, Sep. 2022, doi: 10.1109/JSEN.2022.3192552.
- [15] X. Niu, H. Tang, T. Zhang, J. Fan, and J. Liu, “IC-GVINS: A Robust, Real-Time, INS-Centric GNSS-Visual-Inertial Navigation System,” *IEEE Robot. Autom. Lett.*, vol. 8, no. 1, pp. 216–223, Jan. 2023, doi: 10.1109/LRA.2022.3224367.
- [16] M. Grupp, “evo.” Mar. 2023. [Online]. Available: <https://github.com/MichaelGrupp/evo>
- [17] Z. Zhang and D. Scaramuzza, “A Tutorial on Quantitative Trajectory Evaluation for Visual(-Inertial) Odometry,” in *2018 IEEE/RSJ International Conference on Intelligent Robots and Systems (IROS)*, Madrid: IEEE, Oct. 2018, pp. 7244–7251. doi: 10.1109/IROS.2018.8593941.
- [18] V. Lepetit, F. Moreno-Noguer, and P. Fua, “EPnP: An Accurate O(n) Solution to the PnP Problem,” *Int. J. Comput. Vis.*, vol. 81, no. 2, pp. 155–166, Feb. 2009, doi: 10.1007/s11263-008-0152-6.